Variable Name	Description	Unit	File
LAT	latitude (cell centers)	degree	GRIDBDY2D, GRIDCRO2D
LON	longitude (cell centers)	degree	GRIDBDY2D, GRIDCRO2D
MSFX2	squared map-scale factor (cell centers)	$m^2\ m^{-2}$	GRIDBDY2D, GRIDCRO2D
HT	terrain elevation	m	GRIDBDY2D, GRIDCRO2D
DLUSE	dominant land use	category	GRIDBDY2D, GRIDCRO2D
LWMASK	land-water mask	category	GRIDBDY2D, GRIDCRO2D
PURB	urban percent of cell based on land coverage	percent	GRIDBDY2D, GRIDCRO2D
LUFRAC	fraction of land use by category	unitless	GRIDBDY2D, GRIDCRO2D
LATD	latitude (cell corners)	degree	GRIDDOT2D
LOND	longitude (cell corners)	degree	GRIDDOT2D
MSFD2	squared map scale factor (cell corners)	$m^2\ m^{-2}$	GRIDDOT2D
LATU	latitude (cell west-east faces)	degree	GRIDDOT2D
LONU	longitude (cell west-east faces)	degree	GRIDDOT2D
MSFU2	squared map scale factor (cell west-east faces)	$m^2\ m^{-2}$	GRIDDOT2D
LATV	latitude (cell south-north faces)	degree	GRIDDOT2D
LONV	longitude (cell south-north faces)	degree	GRIDDOT2D
MSFV2	squared map scale factor (cell south-north faces)	$m^2\ m^{-2}$	GRIDDOT2D
JACOBF	total Jacobian (layer face)	m	METBDY3D, METCRO3D
JACOBM	total Jacobian (layer middle)	m	METBDY3D, METCRO3D
DENSA_J	Jacobian-weighted total air density	$kg\ m^{-2}$	METBDY3D, METCRO3D

WHAT_JD	Jacobian- and density-weighted vertical contravariant velocity	kg m^{-1} s^{-1}	METBDY3D, METCRO3D
TA	air temperature	K	METBDY3D, METCRO3D
QV	water vapor mixing ratio	kg kg^{-1}	METBDY3D, METCRO3D
PRES	air pressure	Pa	METBDY3D, METCRO3D
DENS	air density	kg m^{-3}	METBDY3D, METCRO3D
ZH	mid-layer height above ground	m	METBDY3D, METCRO3D
ZF	full layer height above ground	m	METBDY3D, METCRO3D
QC	cloud water mixing ratio	kg kg^{-1}	METBDY3D, METCRO3D
QR	rain water mixing ratio	kg kg^{-1}	METBDY3D, METCRO3D
CFRAC_3D	3D resolved cloud fraction	unitless	METBDY3D, METCRO3D
PRSFC	surface pressure	Pa	METCRO2D
USTAR	cell-averaged horizontal friction velocity	m s^{-1}	METCRO2D
WSTAR	convective velocity scale	m s^{-1}	METCRO2D
PBL	planetary boundary layer height	m	METCRO2D
ZRUF	surface roughness length	m	METCRO2D
MOLI	inverse Monin-Obukhov length	m^{-1}	METCRO2D
HFX	sensible heat flux	W m^{-2}	METCRO2D
LH	latent heat flux	W m^{-2}	METCRO2D
RADYNI	inverse aerodynamic resistance	m s^{-1}	METCRO2D
RSTOMI	inverse bulk stomatal resistance	m s^{-1}	METCRO2D
TEMPG	skin temperature at ground	K	METCRO2D
TEMP2	2-m temperature	K	METCRO2D
Q2	2-m water vapor mixing ratio	m s^{-1}	METCRO2D

WSPD10	10-m wind speed	m s^{-1}	METCRO2D
WDIR10	10-m wind direction	degree	METCRO2D
GLW	longwave radiation at ground	W m^{-2}	METCRO2D
RGRND	solar radiation absorbed at ground	W m^{-2}	METCRO2D
RN	non-convective precipitation over interval	cm	METCRO2D
RC	convective precipitation over interval	cm	METCRO2D
CFRAC	total column integrated cloud fraction	unitless	METCRO2D
CLDT	cloud layer top height	m	METCRO2D
CLDB	cloud layer bottom height	m	METCRO2D
WBAR	average liquid water content of cloud	g m^{-3}	METCRO2D
SNOCOV	snow cover	category	METCRO2D
VEG	vegetation coverage	unitless	METCRO2D
LAI	leaf-area index	m^2 m^{-2}	METCRO2D
SEAICE	sea ice	unitless	METCRO2D
WR	canopy moisture content	m	METCRO2D
SOIM1	volumetric soil moisture in near-surface soil	m^3 m^{-3}	METCRO2D
SOIM2	volumetric soil moisture in deep soil	m^3 m^{-3}	METCRO2D
SOIT1	soil temperature in near-surface soil	K	METCRO2D
SOIT2	soil temperature in deep soil	K	METCRO2D
SLTYP	soil texture type	category	METCRO2D
UWIND	u-component of horizontal wind (cell corners)	m s^{-1}	METDOT3D
VWIND	v-component of horizontal wind (cell corners)	m s^{-1}	METDOT3D
UHAT_JD	contravariant U-component wind×density×Jacobian	kg m^{-1} s^{-1}	METDOT3D
VHAT_JD	contravariant V-component wind×density×Jacobian	kg m^{-1} s^{-1}	METDOT3D
UWINDC	u-component of horizontal wind (west-east cell faces)	m s^{-1}	METDOT3D
VWINDC	v-component of horizontal wind (south-north cell faces)	m s^{-1}	METDOT3D

Table S1: MCIP output variables

File Name	Description	Time-Dependence	Spatial Dimensions
GRIDCRO2D	2-D time-independent fields at cell centers	Independent	X*Y
GRIDBDY2D	2-D time-independent fields on domain perimeter	Independent	Perimeter*Z
GRIDDOT2D	2-D time-independent fields at cell corners	Independent	(X+1)*(Y+1)
METCRO2D	2-D time-dependent fields at cell centers	Hourly	X*Y
METCRO3D	3-D time-dependent fields at cell centers	Hourly	X*Y*Z
METBDY3D	3-D time-dependent fields on domain perimeter	Hourly	Perimeter*Z
METDOT3D	3-D time-dependent fields at cell corners	Hourly	(X+1)*(Y+1)*Z

Table S2: Output files of MCIP

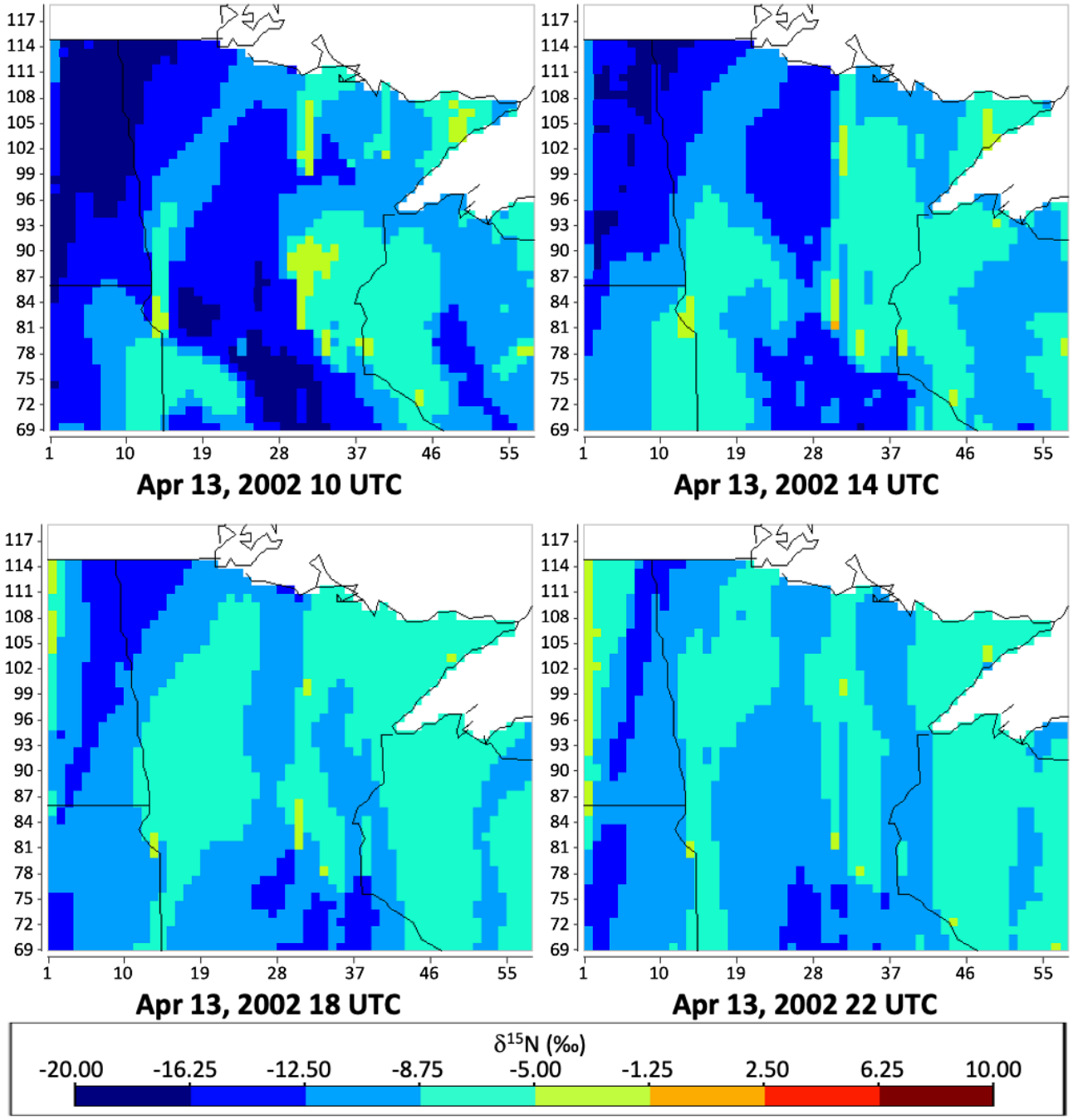

Figure S1: The geographical distribution of the $\delta^{15}N$ value of atmospheric NO_x in per mil (‰) from 10 UTC to 22 UTC on Apr 13, 2002 near the northwest corner of the study domain, simulated by CMAQ, based on NEI-2002 and 2016 meteorology.

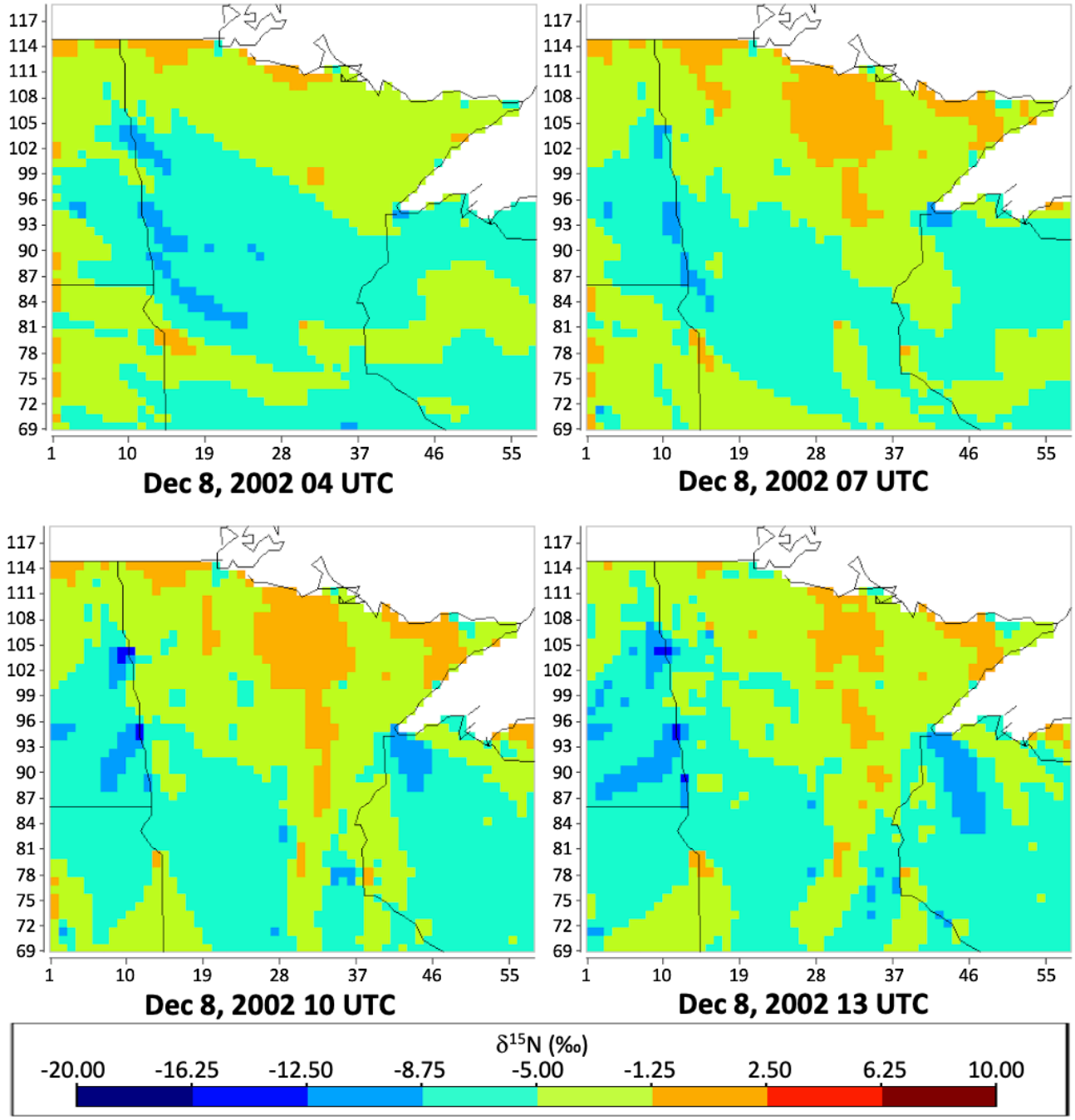

Figure S2: The geographical distribution of the $\delta^{15}N$ value of atmospheric NO_x in per mil (‰) from 04 UTC to 13 UTC on Dec 8, 2002 near the northwest corner of the study domain, simulated by CMAQ, based on NEI-2002 and 2016 meteorology.

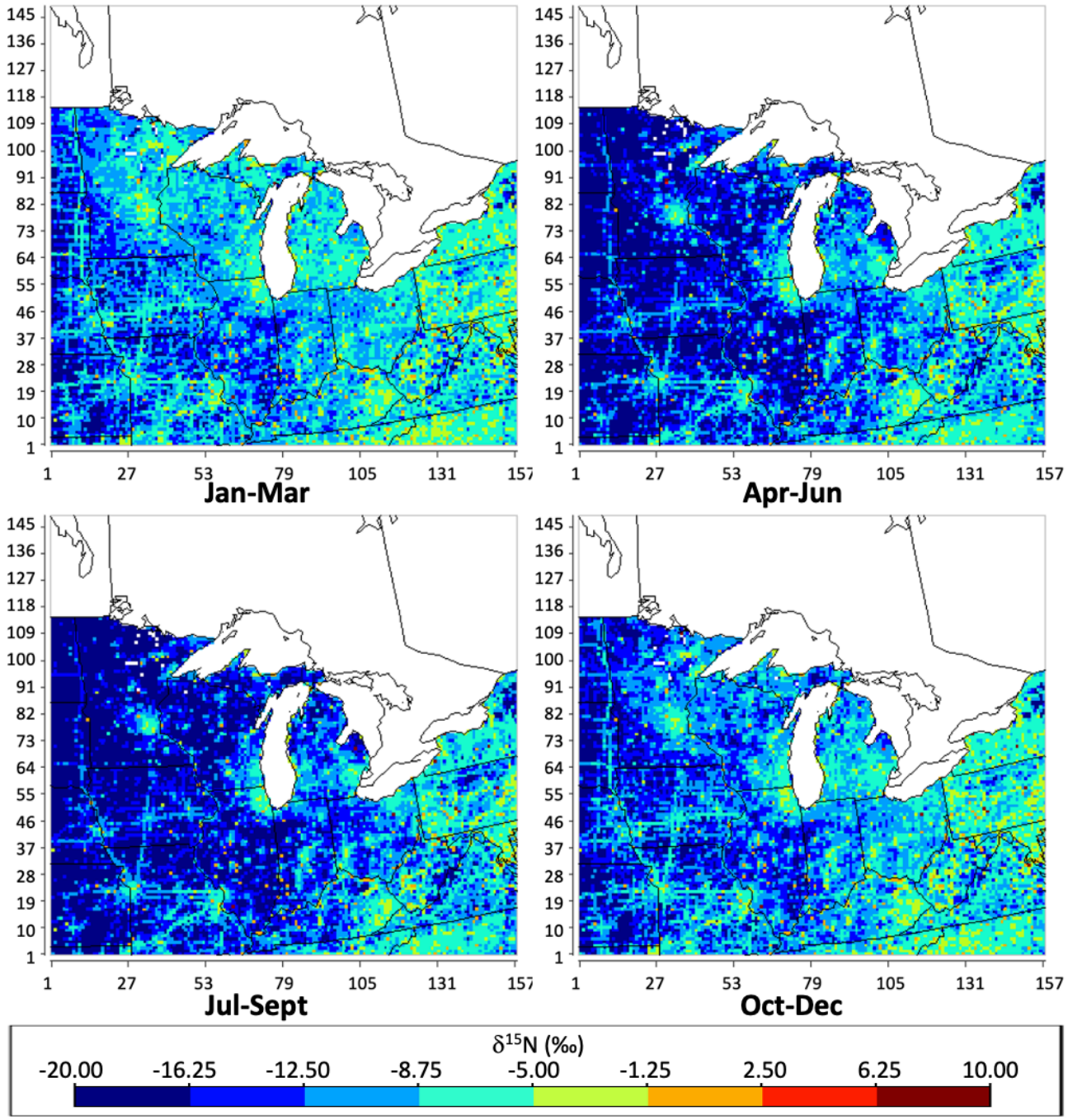

Figure S3: The geographical distribution of the $\delta^{15}N$ value of total NO_x emissions in each season (Winter: Jan-Mar; Spring: Apr-Jun; Summer: Jul-Sep; Fall: Oct-Dec) in per mil (‰) throughout the Midwest simulated by SMOKE, based on NEI-2002.

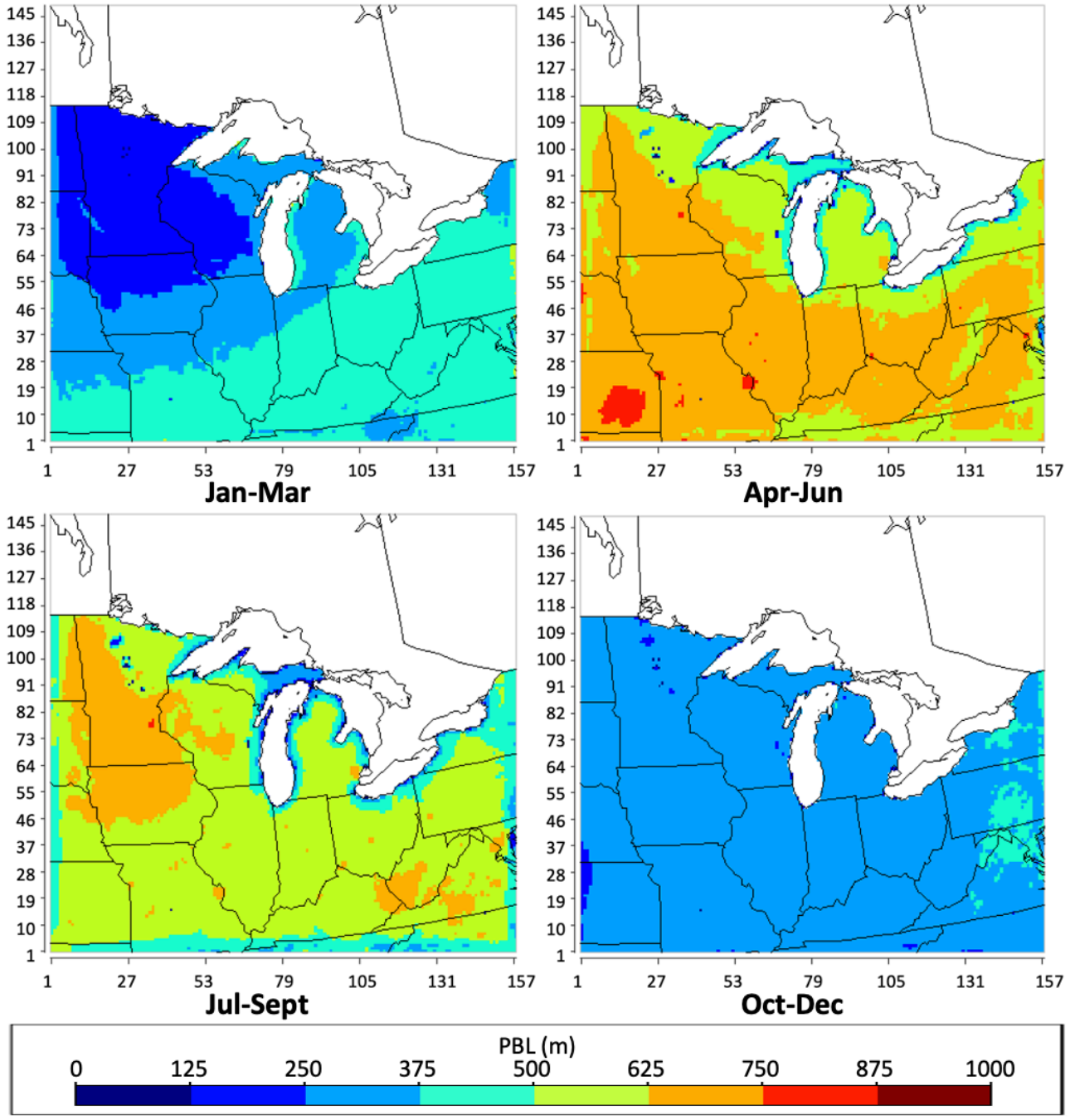

Figure S4: The geographical distribution of the planetary boundary layer (PBL) height in meters during each season (Winter: Jan-Mar; Spring: Apr-Jun; Summer: Jul-Sep; Fall: Oct-Dec) of 2016 throughout the Midwest.

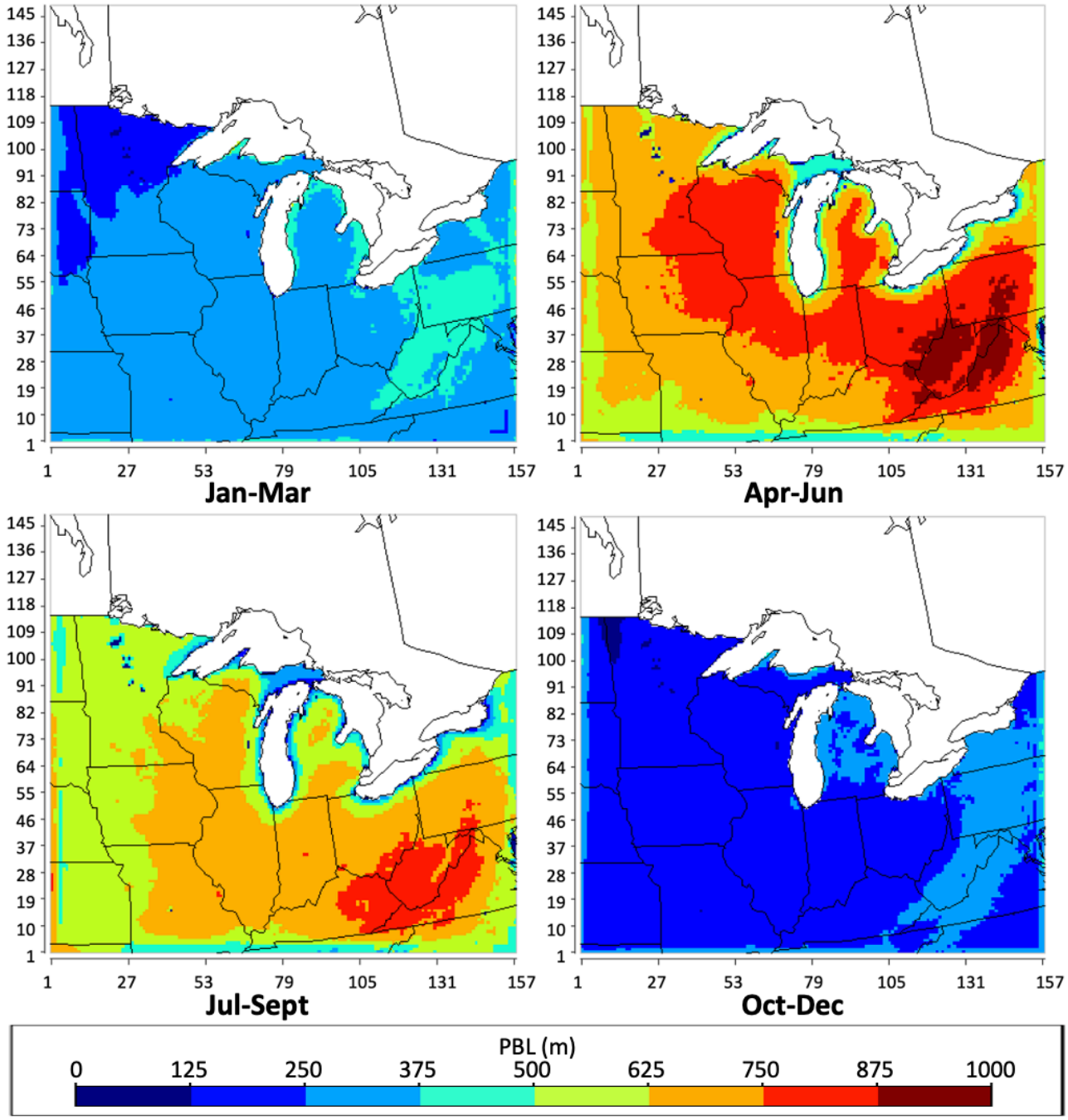

Figure S5: The geographical distribution of the planetary boundary layer (PBL) height in meters during each season (Winter: Jan-Mar; Spring: Apr-Jun; Summer: Jul-Sep; Fall: Oct-Dec) of 2002 throughout the Midwest.

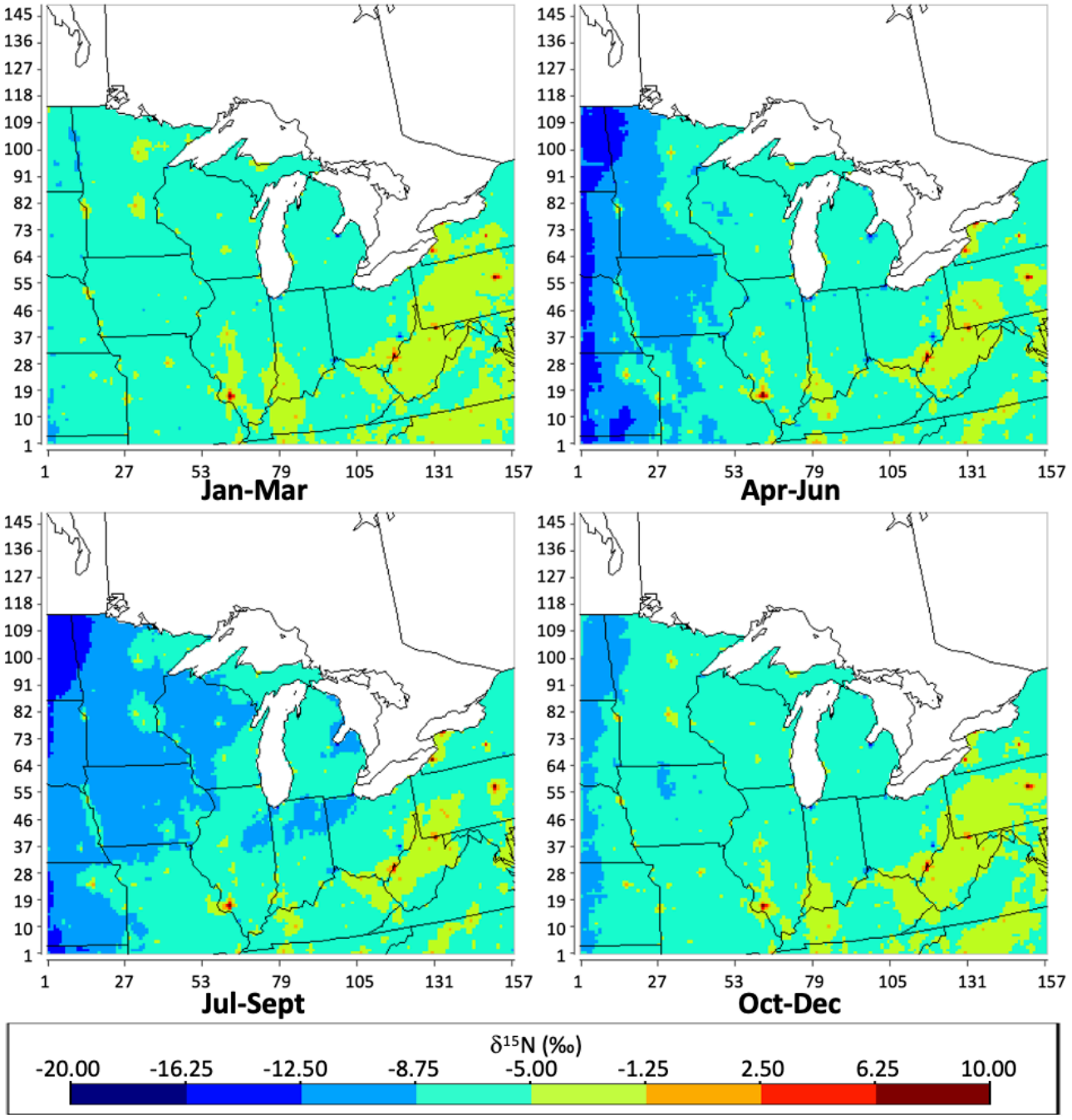

Figure S6: The geographical distribution of the $\delta^{15}N$ value of atmospheric NO_x in each season (Winter: Jan-Mar; Spring: Apr-Jun; Summer: Jul-Sep; Fall: Oct-Dec) in per mil (‰) throughout the Midwest simulated by CMAQ, based on NEI-2002 and 2002 meteorology.

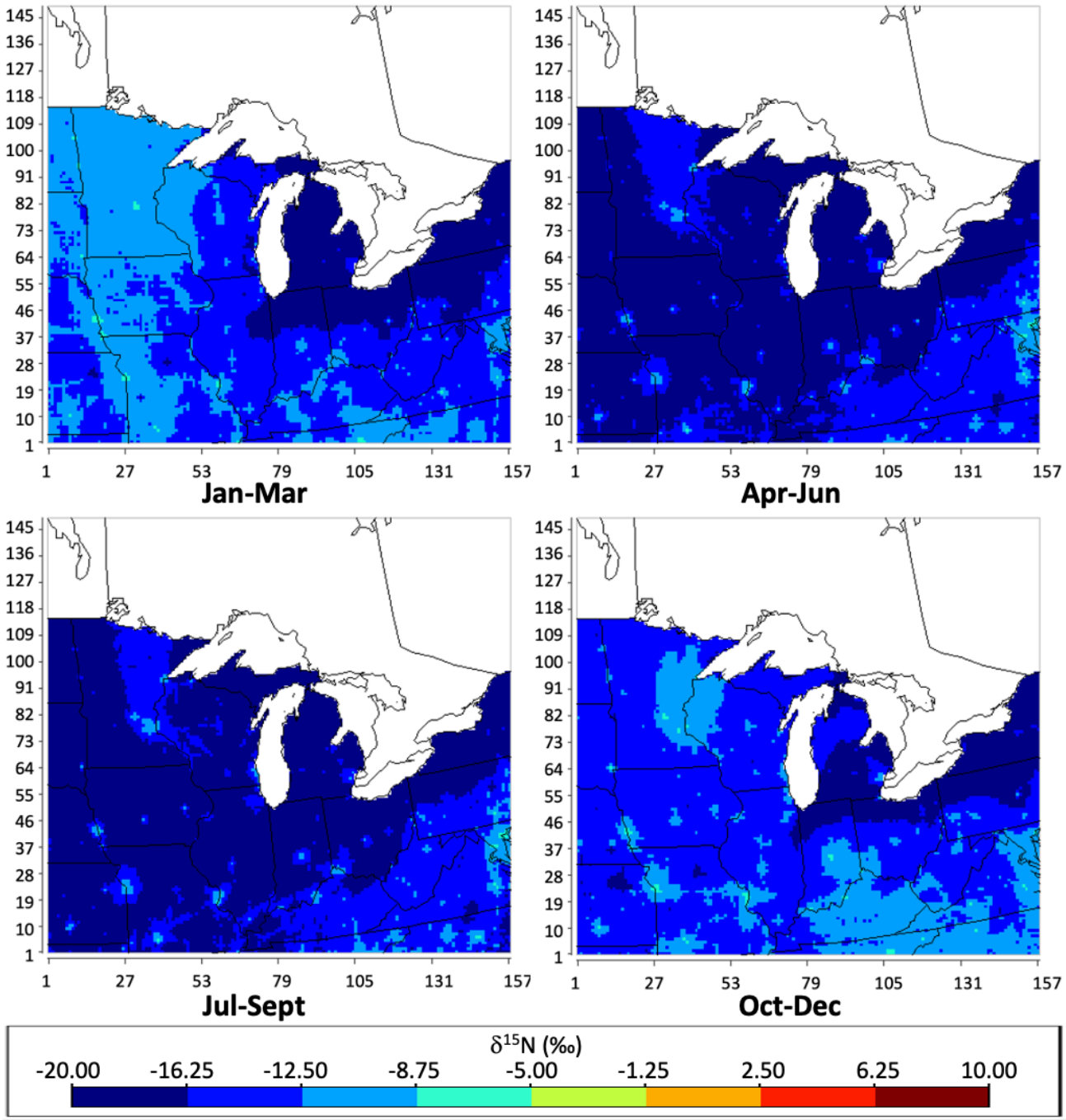

Figure S7: The geographical distribution of the $\delta^{15}N$ value of atmospheric NO_x in each season (Winter: Jan-Mar; Spring: Apr-Jun; Summer: Jul-Sep; Fall: Oct-Dec) in per mil (‰) throughout the Midwest simulated by CMAQ, based on NEI-2016 and 2016 meteorology.

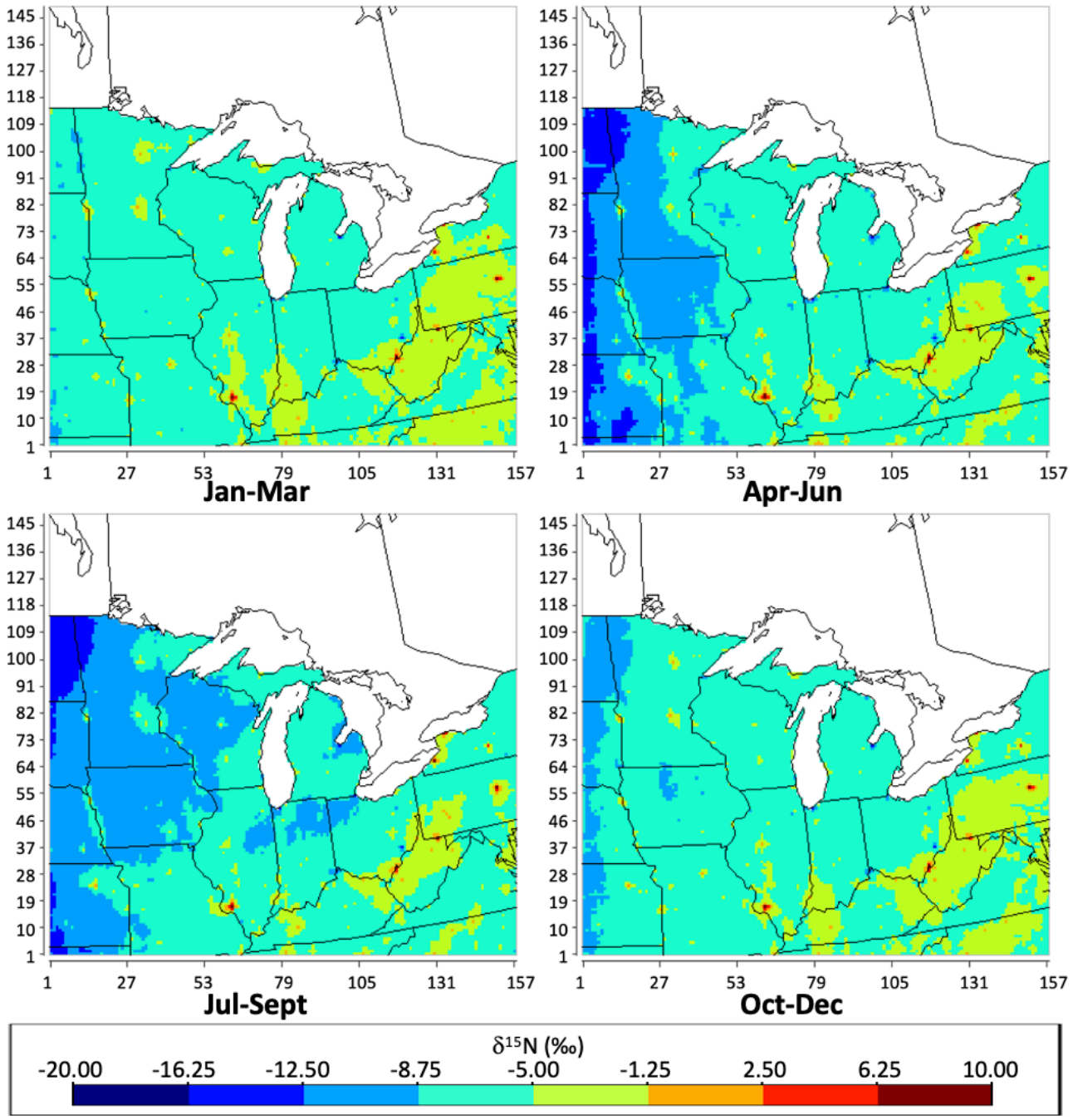

Figure S8: The geographical distribution of the $\delta^{15}N$ value of atmospheric NO_x in each season (Winter: Jan-Mar; Spring: Apr-Jun; Summer: Jul-Sep; Fall: Oct-Dec) in per mil (‰) throughout the Midwest simulated by CMAQ, based on NEI-2002 and 2016 meteorology, under the "amplified deposition" scenario.

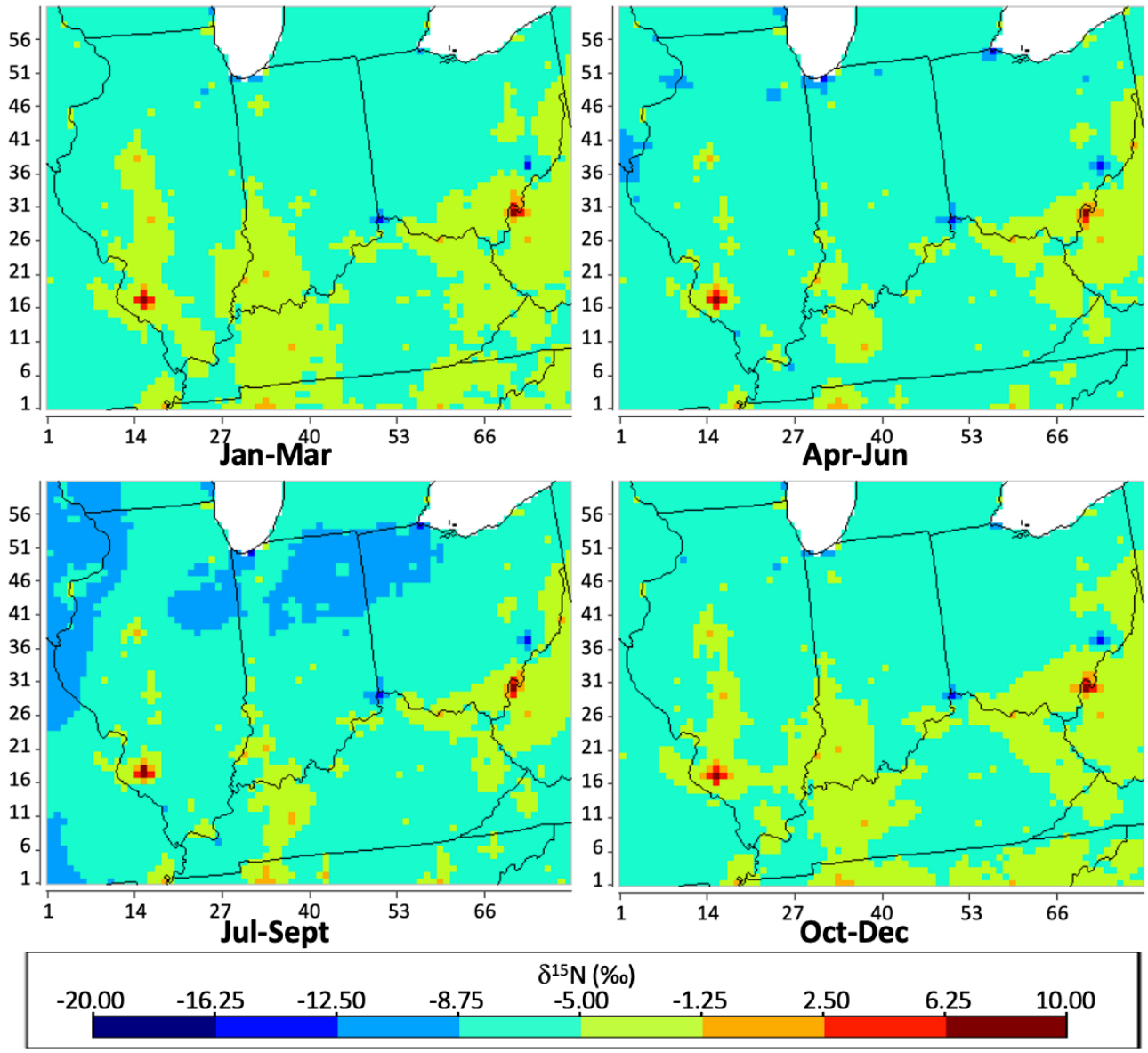

Figure S9: The nested-domain simulation of the $\delta^{15}N$ value of atmospheric NO_x in each season (Winter: Jan-Mar; Spring: Apr-Jun; Summer: Jul-Sep; Fall: Oct-Dec) in per mil (‰) within IN, IL, OH, and KY, based on NEI-2002 and 2016 meteorology.

Site ID	Site Name	County	State	Latitude	Longitude
IN20	Roush Lake	Huntington	IN	40.8401	-85.4639
IN22	Southwest Purdue Agriculture Center	Knox	IN	38.7408	-87.4855
IN34	Indiana Dunes National Lakeshore	Porter	IN	41.6318	-87.0881
IN41	Agronomy Center for Research and Extension	Tippecanoe	IN	40.4749	-86.9924
IL46	Alhambra	Madison	IL	38.8689	-89.6219
IL63	Dixon Springs Agricultural Center	Pope	IL	37.4356	-88.6719
OH09	Oxford	Butler	OH	39.5309	-84.7238
KY19	Cannons Lane	Jefferson	KY	38.2288	-85.6545

Table S3: NADP sites within the states of Indiana, Illinois, Ohio, and Kentucky